the FEBS Journal

Thermal unfolding mechanism of lipocalin-type prostaglandin D synthase

Tsukimi Iida[1], Shigenori Nishimura[2], Maki Mochizuki[2], Susumu Uchiyama[3], Tadayasu Ohkubo[4], Yoshihiro Urade[5], Akiyoshi Tanaka[6] and Takashi Inui[1,2]

1 Department of Food and Nutrition, Tsu City College, Mie, Japan
2 Graduate School of Life and Environmental Sciences, Osaka Prefecture University, Japan
3 Department of Biotechnology, Graduate School of Engineering, Osaka University, Japan
4 Faculty of Pharmaceutical Sciences, Osaka University, Japan
5 Department of Molecular Behavioral Biology, Osaka Bioscience Institute, Japan
6 Faculty of Bioresources, Mie University, Japan

Keywords
differential scanning calorimetry; intermediate; lipocalin; L-PGDS; thermal unfolding

Correspondence
T. Inui, Department of Protein Sciences, Graduate School of Life and Environmental Sciences, Osaka Prefecture University, 1-1 Gakuen-cho, Naka-ku, Sakai, Osaka 599-8531, Japan
Fax: +81 72 254 9474
Tel: +81 72 254 9473
E-mail: inuit@bioinfo.osakafu-u.ac.jp

(Received 6 September 2007, revised 12 November 2007, accepted 15 November 2007)

doi:10.1111/j.1742-4658.2007.06193.x

Lipocalin-type prostaglandin (PG) D synthase (L-PGDS) is a dual-functioning protein in the lipocalin family, acting as a PGD_2-synthesizing enzyme and as an extracellular transporter for small lipophilic molecules. We earlier reported that denaturant-induced unfolding of L-PGDS follows a four-state pathway, including an activity-enhanced state and an inactive intermediate state. In this study, we investigated the thermal unfolding mechanism of L-PGDS by using differential scanning calorimetry (DSC) and CD spectroscopy. DSC measurements revealed that the thermal unfolding of L-PGDS was a completely reversible process at pH 4.0. The DSC curves showed no concentration dependency, demonstrating that the thermal unfolding of L-PGDS involved neither intermolecular interaction nor aggregation. On the basis of a simple two-state unfolding mechanism, the ratio of van't Hoff enthalpy (ΔH_{vH}) to calorimetric enthalpy (ΔH_{cal}) was below 1, indicating the presence of an intermediate state (I) between the native state (N) and unfolded state (U). Then, statistical thermodynamic analyses of a three-state unfolding process were performed. The heat capacity curves fit well with a three-state process; and the estimated transition temperature (T_m) and enthalpy change (ΔH_{cal}) of the $N \leftrightarrow I$ and $I \leftrightarrow U$ transitions were 48.2 °C and 190 $kJ \cdot mol^{-1}$, and 60.3 °C and 144 $kJ \cdot mol^{-1}$, respectively. Correspondingly, the thermal unfolding monitored by CD spectroscopy at 200, 235 and 290 nm revealed that L-PGDS unfolded through the intermediate state, where its main chain retained the characteristic β-sheet structure without side-chain interactions.

Lipocalin-type prostaglandin (PG) D synthase (L-PGDS, prostaglandin-H_2 D-isomerase, EC 5.3.99.2) is the key enzyme responsible for the formation of PGD_2, and is abundantly expressed in the central nervous system and male genitals of various mammals, as well as in the human heart [1,2]. PGD_2 acts as a neuromodulator in the central nervous system, where it induces sleep and regulates body temperature, luteinizing hormone release, and pain responses [1]. In the peripheral tissues, PGD_2 induces vasodilation and bronchoconstriction [3,4], and acts as a mediator of allergy and inflammatory responses [1,5]. On the other hand, L-PGDS is a member of the lipocalin superfamily [6], which comprises lipid-transporter proteins such as β-lactoglobulin (β-LG) and retinol-binding protein [7]. The lipocalins are particularly interesting because

Abbreviations
DSC, differential scanning calorimetry; I, intermediate state; L-PGDS, lipocalin-type prostaglandin D synthase; N, native state; PG, prostaglandin; U, unfolded state; β-LG, β-lactoglobulin.

of their wide range of functions and high levels of sequence divergence with closely similar folds. All have a similar structure, including a conserved ligand-binding hydrophobic cavity. They are a family of diverse proteins that normally serve for the storage or transport of physiologically important lipophilic ligands [8,9], and it is becoming increasingly clear that some of them have many other important functions, such as the modulation of cell growth and metabolism [10]. L-PGDS also has the ability to bind retinoids, bile pigments such as bilirubin and biliverdin, thyroid hormones, gangliosides, and amyloid β-peptide *in vitro* [11–15]. Thus, L-PGDS is a dual-functioning protein in the lipocalin family, acting as both a PGD_2-synthesizing enzyme and an extracellular transporter protein for lipophilic ligands.

A great deal is known about the structural mechanisms of unfolding in several different systems, ranging from simple model proteins to modular proteins. Understanding the structure–function relationships of a protein under different conditions is fundamentally important for both theoretical and applied aspects. For example, insight into the molecular basis of protein stability can aid in the design of artificial proteins with special properties for biotechnological applications. In a previous study, we characterized the unfolding process of L-PGDS in the presence of denaturants such as guanidine hydrochloride and urea [16]. We found that L-PGDS unfolds from its native to completely unfolded state through two different states, an activity-enhanced state at a low concentration of denaturants, and an inactive intermediate at a higher concentration of denaturants; therefore, we proposed a four-state (equilibrium) unfolding model for L-PGDS. L-PGDS is a good tool for understanding the structure–function relationships in the lipocalin family, that is, the correlation between structural changes in it and its dual functions of enzyme activity and ligand binding. Such a characteristic of L-PGDS during the unfolding process in the presence of denaturants prompted us to study the thermal stability of L-PGDS, as thermodynamic characterization of the structural transition of a protein is fundamentally important for understanding the folding mechanisms and the interactions that stabilize the native state [17]. In comparison to those of other small globular proteins, however, very few structural and thermodynamic data are available for the lipocalin superfamily.

The combination of differential scanning calorimetry (DSC) measurement and data obtained with structural probes, such as CD, is a powerful approach for studying protein folding and unfolding. Such an approach makes it possible to correlate the thermodynamic parameters obtained by the measurements of DSC and CD and to detect and characterize possible intermediate states. In the present study, we investigated the thermal unfolding of L-PGDS by the use of DSC and CD. On the basis of the thermodynamic and structural characterization of the states during the unfolding process of L-PGDS, we proposed three-state unfolding through an intermediate state, where the secondary structure is still maintained.

Results

DSC profiles of L-PGDS

First, the heat capacity curve of L-PGDS was acquired at pH 8.0, a pH at which the enzymatic activity of L-PGDS had been examined previously. As shown in Fig. 1, a distorted exothermal reaction was observed at around 70 °C, indicating the aggregation of unfolded L-PGDS. Rescanning of the sample solution after heating at 80 °C resulted in no calorimetric transition, showing that the unfolding at pH 8.0 was an irreversible reaction (data not shown). Similarly, at pH 5.0 and pH 6.0, both DSC traces at initial scanning undershot the completion of the unfolding, most probably due to precipitation (Fig. 1). At pH 4.0, however, a single endothermic peak corresponding to the thermal unfolding of L-PGDS was observed at around 50 °C. The thermal unfolding started in the vicinity of 20 °C, had a peak at 50 °C, and was completed in the vicinity of 80 °C. In order to investigate the reversibility of the thermal unfolding at pH 4.0, an L-PGDS solution

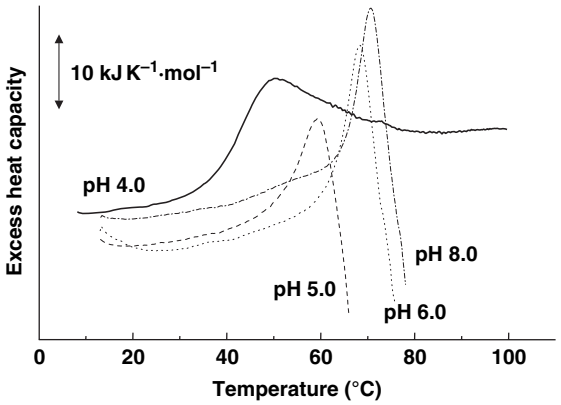

Fig. 1. Thermogram profiles of L-PGDS. The DSC traces for the unfolding of L-PGDS were obtained at pH 4.0 (solid line), pH 5.0 (dashed line), pH 6.0 (dotted line) and pH 8.0 (dot-dashed line) in 20 mM of several buffers. The scan rate of DSC was 1 °C·min^{-1}, and the protein concentration was 1 mg·mL^{-1}. Baseline-subtracted data have been normalized for protein concentration.

after the initial scanning up to 100 °C was cooled to 20 °C in the calorimeter cell and subsequently rescanned. The rescanned DSC curve was almost the same as the initial curve, demonstrating that the thermal unfolding of L-PGDS was reversible at pH 4.0.

Concentration dependence of L-PGDS thermal unfolding

Next, we investigated the dependence of the thermal unfolding profile on the concentration of L-PGDS. The protein concentrations used were 0.25, 0.5 and 1 mg·mL^{-1}. All traces showed a single endothermic peak at around 50 °C, with no concentration dependence of the peak temperature (Fig. 2). These results show that the thermal unfolding of L-PGDS involved neither dissociation nor association.

Deconvolution of L-PGDS thermal unfolding

Assuming the two-state unfolding process of L-PGDS from the native state (N) to the unfolded state (U), we calculated the ratio between the molar calorimetric enthalpy change and the van't Hoff enthalpy change ($\Delta H_{vH}/\Delta H_{cal}$) to be 0.5 [Eqns (1,2) in Experimental procedures]. This result indicates that the thermal unfolding of L-PGDS cannot be explained as a simple two-state process and implies the presence of unfolding intermediate states (I) [18].

Nonlinear least-squares fitting with the three-state equilibrium unfolding model (N ↔ I ↔ U) was then applied to the heat capacity curve, which gave an excellent fit (Fig. 3). The values of thermodynamic parameters were calculated by the use of the theoretical model [Eqns (5–13) in Experimental procedures]. The transition temperature (T_m) and ΔH of N ↔ I and of I ↔ U were 48.0 °C and 206 kJ·mol^{-1}, and 60.8 °C and 163 kJ·mol^{-1}, respectively; and the values for other parameters are listed in Table 1. Using these parameters, we estimated the population of each state of L-PGDS as a function of temperature [data not shown, Eqns (3–5) in Experimental procedures]. The intermediate state reached a maximum population of about 65% at 53.9 °C, and took an equal value to the unfolded population at 60.8 °C. Figure 4 shows the variation of ΔG, ΔH and $-T\Delta S$ as a function of the temperature for both thermal transitions, N ↔ I and I ↔ U. On both transitions, ΔH and $-T\Delta S$ increased and decreased, respectively, with increase in temperature. Concerning ΔH, ΔH_{NI} was higher than ΔH_{IU}. The temperature dependence of ΔG of both transitions (ΔG_{NI} and ΔG_{IU}) indicates that both the native and intermediate L-PGDS is most stable at a temperature below 0 °C.

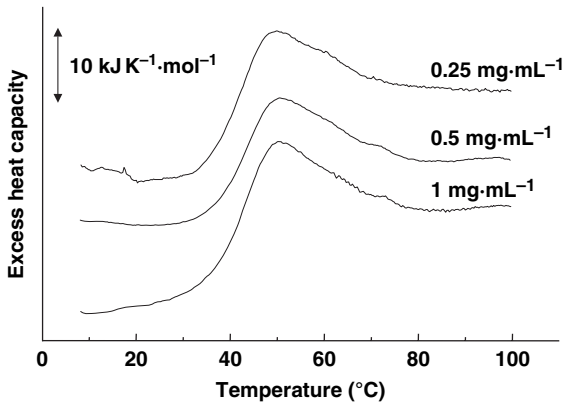

Fig. 2. Concentration dependence of thermal unfolding of L-PGDS. The DSC traces of L-PGDS were measured at pH 4.0. The protein concentrations were 0.25, 0.5, and 1 mg·mL^{-1} (values shown above curves). Results of DSC experiments are shown as heat capacity versus temperature profiles.

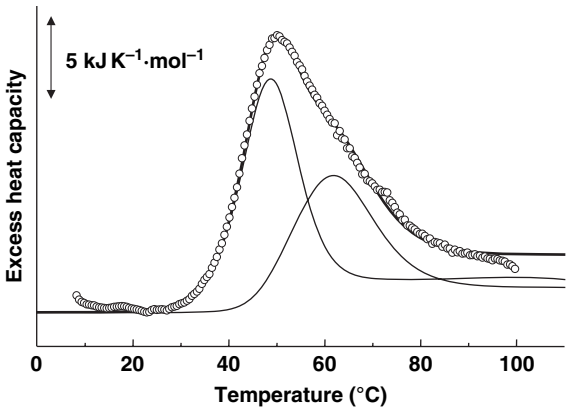

Fig. 3. DSC curve deconvolution for thermal unfolding of L-PGDS. A sequential three-state transition model, N ↔ I ↔ U. Open circle, observed DSC data; solid line, component curves; and dotted line, theoretical curve.

Thermal unfolding of L-PGDS observed by far-UV and near-UV CD spectra

Next, to obtain insight into the structural changes, we followed the heat-induced unfolding transition of L-PGDS by using far-UV and near-UV CD. The equilibrium CD spectra of L-PGDS at various temperatures were measured in the far-UV and near-UV regions at pH 4.0, at which the thermal unfolding was confirmed as a thermodynamically reversible process from the results of the DSC measurements (Figs 1–3). The far-UV spectrum of the native L-PGDS at 20 °C

Table 1. Thermodynamic parameters for unfolding of L-PGDS obtained by DSC measurements. T_m, ΔH, ΔS, ΔC_p and ΔG denote transition temperature, enthalpy change, entropy change, heat capacity change, and Gibbs free energy change from N to I and from I to U, respectively.

Step	T_m (°C)	$\Delta H(T_m)$ (kJ·mol^{-1})	$\Delta S(T_m)$ (kJ·K^{-1}·mol^{-1})	ΔC_p (kJ·K^{-1}·mol^{-1})	ΔG (298.15 K) (kJ·mol^{-1})
N ↔ I	48.0 ± 0.1	206 ± 2	0.64 ± 0.1	2.0 ± 0.1	13 ± 0.2[a]
I ↔ U	60.8 ± 0.1	163 ± 2	0.49 ± 0.1	1.7 ± 0.1	15 ± 0.2[b]

[a] This value corresponds to ΔG_{NI}, which is equal to ΔG_I. [b] This value corresponds to ΔG_{IU}, which is equal to $\Delta G_U - \Delta G_I$. Errors were estimated on the basis of the lack of certainty regarding heat capacity values.

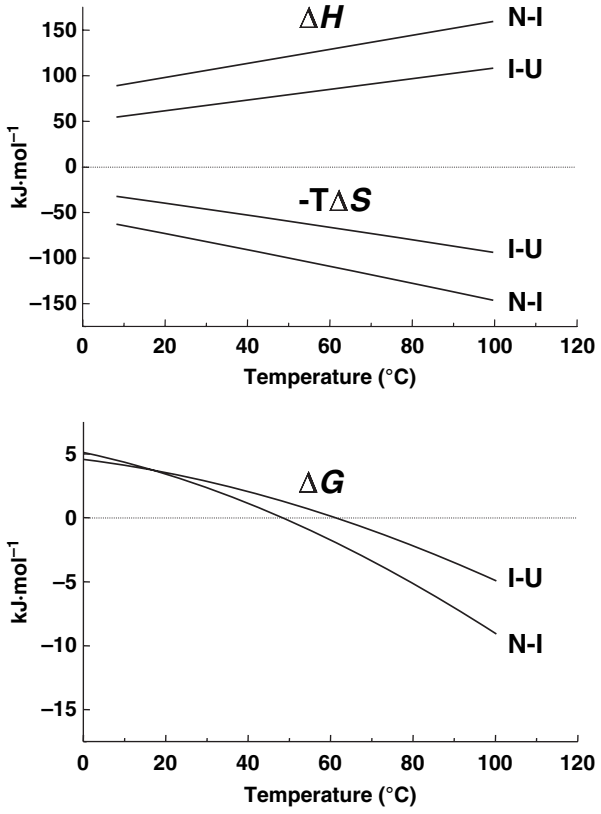

Fig. 4. Enthalpy, entropy and Gibbs energy changes for the N ↔ I transition and the I ↔ U transition of L-PGDS.

showed a spectrum with an abundance of β-sheet structure (Fig. 5A), which represents a structural feature of L-PGDS. At 40 °C, the CD spectrum still showed an abundance of this β-sheet structure. Then, unordered conformation was increased gradually up to 80 °C. The near-UV CD spectrum of the native L-PGDS at 20 °C exhibited Cotton effects, with negative maxima at 284, 286 and 290 nm, and positive maxima at 260, 268 and 272 nm, indicating the anisotropic environment of the aromatic side chains in the native state (Fig. 5B). These Cotton effects disappeared upon thermal unfolding. Furthermore, the CD spectrum remeasured at 20 °C after the sample had been heated to 90 °C was almost identical to that observed at the initial measurement, demonstrating that the thermal unfolding of L-PGDS at pH 4.0 was also structurally reversible.

Figure 6 shows the equilibrium transition curves of L-PGDS monitored at 200, 235 and 290 nm, at which wavelengths the change in ellipticity was larger. The transition temperature, T_m and van't Hoff enthalpy change, $\Delta H(T_m)$, were obtained by fitting according to Eqns (14–16) in Experimental procedures. As it was difficult to evaluate the ΔC_p value in this calculation because of the scattered data, ΔC_p values obtained by DSC measurements were used (Table 1). Fitting of the data obtained at 200 and 235 nm to a model for two-state equilibrium folding showed a T_m of 54.6 ± 0.4 °C and a $\Delta H(T_m)$ of 128 ± 6 kJ·mol^{-1} for the transition at 200 nm, and a T_m of 47.3 ± 0.1 °C and a $\Delta H(T_m)$ of 228 ± 7 kJ·mol^{-1} at 235 nm (Fig. 6, Table 2). The data obtained at 290 nm were fitted to a two-state model by using only the data obtained between 20 °C and 70 °C. T_m and $\Delta H(T_m)$ for the transition at 290 nm were 46.9 ± 0.1 °C and 262 ± 6 kJ·mol^{-1}, respectively. The thermodynamic parameters are summarized in Table 2, and the fitting curves calculated with these parameters are shown as solid lines in Fig. 6.

Discussion

In this study, both DSC and CD measurements revealed that L-PGDS reversibly unfolded at pH 4.0 through an intermediate state upon a temperature increase. The thermal unfolding of L-PGDS was analyzed by a two-state or a three-state equilibrium unfolding model, and the calculated values for the thermodynamic parameters were summarized (Tables 1 and 2). Although the thermodynamic parameters obtained by CD spectroscopy did not show complete agreement with those obtained by DSC measurement, the comparison of the thermodynamic parameters provided structural insights into the observed unfolding. The transition monitored by CD spectroscopy at both 235 and 290 nm could be assumed to correspond to

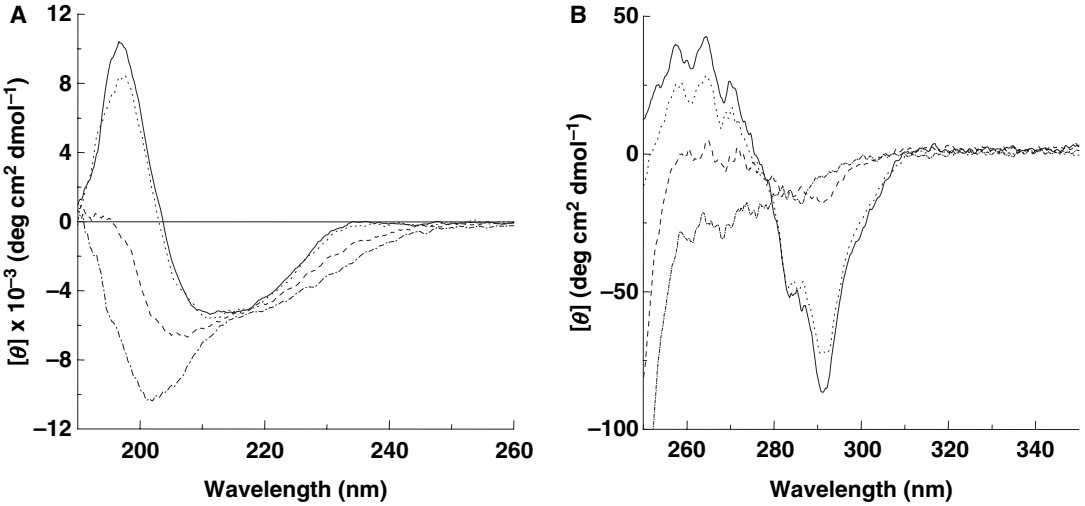

Fig. 5. (A) Far-UV (190–260 nm) and (B) near-UV (250–350 nm) CD spectra at various temperatures of L-PGDS at pH 4.0. The CD spectra of L-PGDS were obtained at 20 °C (solid line), 40 °C (dotted line), 60 °C (dashed line), and 80 °C (dot-dashed line).

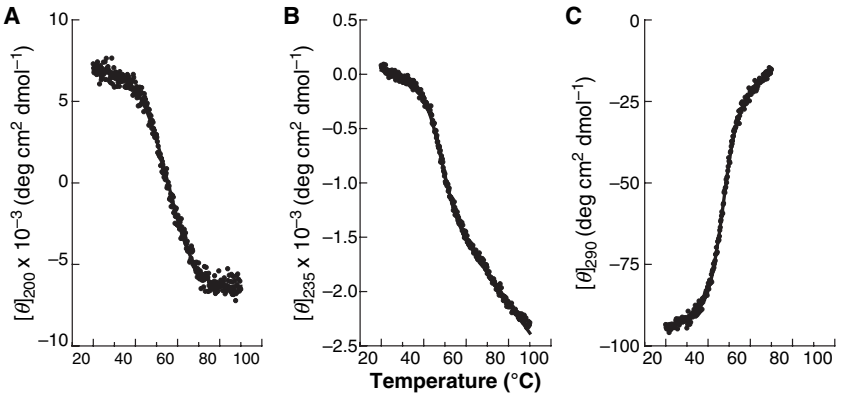

Fig. 6. Thermal unfolding curves of L-PGDS at pH 4.0. Unfolding transitions were monitored by measurement of CD at 200 (A), 235 (B), and 290 nm (C). The curves are the fitting curves based on experimental points by nonlinear least-squares analysis for the two-state transition according to Eqns (14–16).

Table 2. Thermodynamic parameters for unfolding of L-PGDS obtained by CD measurements.

Wavelength (nm)	T_m (°C)	$\Delta H(T_m)$ (kJ·mol^{-1})
200	54.6 ± 0.4	128 ± 6
235	47.3 ± 0.1	228 ± 6
290	46.9 ± 0.1	262 ± 6

the native state to heat-induced intermediate state (I_h) transition. It is well known that the contribution from aromatic side-chain conformation can potentially alter the overall far-UV CD signal in proteins [19]. Thus, the $N \leftrightarrow I_h$ transition is considered to reflect a change in the environment of the aromatic side chains. In contrast, the changes in secondary structure monitored at 200 nm apparently showed two-state equilibrium unfolding, and the transition was assumed to correspond to the I_h to heat-induced unfolded state (U_h) transition. Moreover, in our recent fluorescence quenching experiments designed to investigate the ability of L-PGDS to bind biliverdin, a lipophilic small ligand, during the thermal unfolding process, this binding ability of L-PGDS was still retained at 55 °C and pH 4.0 (T. Iida and T. Inui, unpublished results). In the present study, we showed that the population of L-PGDS in the heat-induced intermediate state became maximal at 53.9 °C. These results, taken together, demonstrate that the tertiary structure of L-PGDS became disrupted prior to the collapse of the secondary structure, and thus suggest that the thermal intermediate of L-PGDS still maintained a significant amount of the secondary structure found in the native state that has a function as a transporter protein for small lipophilic ligands.

On the basis of the results of our previous study on chemically induced unfolding of L-PGDS by using a denaturant such as guanidine hydrochloride or urea,

we proposed a four-state equilibrium unfolding model for L-PGDS that included a denaturant-induced activity-enhanced state and denaturant-induced inactive intermediate state. In this scheme, both the denaturant-induced activity-enhanced state and denaturant-induced inactive intermediate state are located on a sequential pathway from the native to denaturant-induced unfolded state, and they are associated with changes in the enzyme activity representing both activation and inactivation, respectively. Chemical denaturant-induced unfolding of L-PGDS was performed at pH 8.0, which gave the maximum enzymatic activity, whereas the heat-induced unfolding of L-PGDS was performed at pH 4.0, where complete reversibility was ensured. At 20 °C, the far-UV CD spectrum measured at pH 4.0 was almost identical to that measured at pH 8.0 (data not shown), suggesting that L-PGDS at pH 4.0 was still stable and maintained the same secondary structure as obtained at pH 8.0. However, the far-UV CD spectrum obtained at 90 °C under the acidic condition was completely different from that obtained in the presence of 6 M urea at pH 8.0, demonstrating that the heat-induced structure of the heat-induced unfolded state was different from the structure of the denaturant-induced unfolded state (Fig. 5A) [16]. In case of denaturant-induced unfolding, the tertiary structure of L-PGDS completely disappeared, whereas in the case of heat-induced unfolding, the secondary structure of L-PGDS was retained. So far, in many cases, thermally denatured proteins have shown a higher degree of preservation of their secondary structure than chemically denatured proteins [20,21]. With regard to the structure of the intermediate, we suggest that the denaturant-induced inactive intermediate state of L-PGDS was in a molten globule-like state, because it contained a pronounced secondary structure without a rigid tertiary structure and apparent L-PGDS function [16]. Thus, the structure of the denaturant-induced inactive intermediate state was considered to be different from that of the heat-induced intermediate state. These results, taken together, indicate that the unfolding mechanism was completely different between these two unfolding processes. Further investigations are necessary to clarify both the heat-induced and denaturant-induced unfolding processes of L-PGDS. Multidimensional NMR or small-angle X-ray scattering coupled with DSC will help to identify the structure of the intermediate of L-PGDS.

In the lipocalin superfamily, which consists of a β-barrel of eight continuous antiparallel β-strands as their central motif, β-LG is one of the well-characterized proteins used in studies concerning protein folding and unfolding [22–24]. Bovine β-LG is acid-stable and maintains its barrel fold at pH values as low as 2, where it assumes the monomer state, showing disordered conformations only at the level of loops [25–27]. Most recently, we showed that the structure of mouse recombinant L-PGDS exhibited the typical lipocalin fold, consisting of an eight-stranded, antiparallel β-barrel and a long α-helix associated with the outer surface of the barrel [28]. In this study, L-PGDS was also very stable at acidic pH, as indicated by the far-UV CD spectral data, suggesting a rigid conformation of β-strands in lipocalin folding. The structural stability over a wide range of pH might be a special feature of lipocalin family proteins.

In summary, on the basis of the thermodynamic characterization of the unfolding of L-PGDS together with the characterization of its structure during the unfolding process, we proposed three-state unfolding through an intermediate state. The secondary structure of the intermediate was the characteristic β-sheet structure without side-chain interactions, and was considered to be completely different from that of the intermediates induced by denaturants [16]. As L-PGDS has the ability to bind small hydrophobic ligands such as retinoids, bile pigments and thyroid hormones *in vitro*, our next task is to investigate possible changes in the thermal stability of L-PGDS caused by the binding of small hydrophobic ligands. We are now planning this experiment and hope to publish the results elsewhere.

Experimental procedures

Expression of recombinant mouse L-PGDS

The full-length cDNA for mouse L-PGDS, which is composed of 189 amino acid residues and has a molecular mass of 18 620 Da (GenBank accession number X89222 [29]), was ligated into the *Bam*HI–*Eco*RI sites of the expression vector pGEX-2T (GE Healthcare Bio-Sciences, Piscataway, NJ, USA). The N-terminal 22 amino acid residues of the signal peptide were deleted. The Cys65 → Ala recombinant enzymes were expressed as a glutathione *S*-transferase fusion protein in *Escherichia coli* DH5α (TOYOBO, Tokyo, Japan), as described previously [16]. The fusion protein was bound to glutathione–sepharose 4B (GE Healthcare Bio-Sciences) and incubated with thrombin (Sigma Chemical Co., St Louis, MO, USA) (100 U per 100 μL) to release the L-PGDS. The recombinant protein was further purified by using size-exclusion chromatography as described previously [13]. Prior to DSC and CD measurements, the protein solutions were dialyzed against the specified buffer for at least 15 h. Buffer solutions used were 20 mM sodium

acetate for the pH 4.0 and pH 5.0 conditions, and 20 mM sodium phosphate for the pH 6.0 and pH 8.0 conditions. The final dialysate was used as a reference for DSC and CD measurements. The protein concentrations were spectrophotometrically determined by using the molar extinction coefficient at 280 nm, ε_{280} = 23 000 $M^{-1}\cdot cm^{-1}$.

Calorimetry

Calorimetric experiments were carried out with a VP-DSC (MicroCal, Northampton, MA, USA) [30]. In addition to the measurements at pH 5.0, 6.0, and 8.0, the protein solutions at concentrations of 0.25, 0.5 and 1.0 $mg\cdot mL^{-1}$ were measured at pH 4.0. All the protein and buffer solutions were degassed with gentle stirring under a vacuum before being loaded into the calorimeter. Experiments were performed over a temperature range of 5–100 °C at a scan rate of 1 $C^{\circ}\cdot min^{-1}$ and excess pressure of 2 atm. Initially, raw DSC data were processed and analyzed with ORIGIN 5.0 software (MicroCal, Northampton, MA, USA), to determine whether the unfolding was a two-state process. Values of thermodynamic parameters for the unfolding were estimated by several methods [18,31–33].

First, the calorimetric enthalpy change at a given temperature, $\Delta H_{cal}(T)$, was estimated simply by the integration of the heat capacity (C_p) after subtraction of the appropriate sigmoidal-shaped baseline, $C_{P,base}$, by using the program ORIGIN 5.0.

$$\Delta H_{cal}(T) = \int_{T_1}^{T} (C_P - C_{P,base})dT \quad (1)$$

where T_1 is the absolute temperature at which the unfolding starts. The total enthalpy change needed for the complete unfolding, ΔH_{cal}, was obtained by integration up to the temperature at which the unfolding was complete. In this case, the unfolding temperature, $T_{1/2}$, was defined as the temperature where $\Delta H_{cal}(T)$ is equal to one-half of the value of ΔH_{cal}. Second, the van't Hoff enthalpy change, ΔH_{vH}, was calculated according to:

$$\Delta H_{vH} = ART_{1/2}^2 C_{P,ex,1/2}/\Delta H_{app} \quad (2)$$

where A has the value 4.00 for a simple two-state unfolding not involving association or dissociation, R is the gas constant, and $C_{P,ex,1/2}$ is the excess heat capacity at $T_{1/2}$ [34–36]. When the ratio of ΔH_{cal} to ΔH_{vH} is exactly the same as unity, the unfolding is considered as a two-state transition [31,35–37].

For the three-state unfolding mechanism, the thermodynamic parameters were estimated from the nonlinear least-squares fitting of excess C_P based on the statistical thermodynamics. The following possible three states were assumed to exist for the unfolding of L-PGDS: N ↔ I ↔ U.

When the native state is defined as the reference state, the populations of the ith state, P_i, are written as

$$P_I = \exp(-\Delta G_I/RT)/\{1 + \exp(-\Delta G_I/RT) + \exp(-\Delta G_U/RT)\} \quad (3)$$

$$P_U = \exp(-\Delta G_U/RT)/\{1 + \exp(-\Delta G_I/RT) + \exp(-\Delta G_U/RT)\} \quad (4)$$

$$P_N = 1 - (P_I + P_U) \quad (5)$$

where ΔG_i is the free energy for each state relative to the reference state (ΔG_N = 0). Then, ΔG_i is written by using intrinsic free energies as:

$$\Delta G_I = \Delta H_I - T\Delta S_I \quad (6)$$

$$\Delta G_U = \Delta H_U - T\Delta S_U \quad (7)$$

where ΔH_i and ΔS_i are the enthalpy and entropy of the ith state relative to the reference state, and are temperature dependent because of the heat capacity change, $\Delta C_{P,i}$:

$$\Delta H_I(T) = \Delta H_I(T_{m,I}) + \Delta C_{P,I}(T - T_{m,I}) \quad (8)$$

$$\Delta H_U(T) = \Delta H_U(T_{m,U}) + \Delta C_{P,U}(T - T_{m,U}) \quad (9)$$

$$\Delta S_I(T) = \Delta H_I(T_{m,I})/T_{m,I} + \Delta C_{P,I}\ln[T/T_{m,I}] \quad (10)$$

$$\Delta S_U(T) = \Delta H_U(T_{m,U})/T_{m,U} + \Delta C_{P,U}\ln[T/T_{m,U}] \quad (11)$$

where $T_{m,I}$ and $T_{m,U}$ are intrinsic transition temperature (transition temperature when no domain–domain interactions exist) for the transition from the native state to the second and third states, respectively. The enthalpy of the system, $H(T)$, is given by the equation:

$$H(T) = P_I\Delta H_I + P_U\Delta H_U \quad (12)$$

As C_P of the system is the differential of enthalpy of the system, $C_P(T)$ is represented by:

$$C_P(T) = dH(T)/dT \quad (13)$$

Substituting from Eqn (5) to Eqn (12) into Eqn (13), the nonlinear least-squares fitting of C_P was performed. Similar treatments of heat capacity curves were previously introduced, in which domain–domain interactions were considered [32,38] or were not considered [33,39]. In the present study, the heat capacity of the native protein, $C_{P,N}$, was assumed to be a linear function of temperature [35,40], and therefore $C_P - C_{P,N}$ is equal to the excess heat capacity. Deconvolution analysis of the excess heat capacity was carried out by using MATHEMATICA 5.1 (Wolfram Research, Champaign, IL, USA), employing the Levenberg–Marquardt algorithm with $T_{m,I}$, $T_{m,U}$, $\Delta C_{P,I}$, $\Delta C_{P,U}$, $\Delta H_I(T_{m,I})$ and $\Delta H_U(T_{m,U})$ as the variables. The heat capacity differences were assumed to be constant and positive [33,39].

CD measurements

The CD spectra of L-PGDS were measured with a spectropolarimeter, model J-820 (Jasco, Tokyo, Japan), equipped with a Peltier PTC-423L thermo-unit (Jasco). For the measurements of far-UV and near-UV equilibrium CD spectra, optical quartz cuvettes with 1.0 and 10 mm path lengths, respectively, were used. The final protein concentrations were 5 and 60 μM for far-UV and near-UV CD measurements, respectively. The measurements were performed at pH 4.0. As for thermal unfolding experiments, changes in the CD intensities were measured at 200, 235 and 290 nm over a temperature range of 20–90 °C at a scan rate of 1 °C·min^{-1}. The path length of the optical cuvette was 10 mm. The final protein concentrations were 0.5, 3.5 and 100 μM for the measurements at 200, 235 and 290 nm, respectively. The data were expressed as molar residue ellipticity (θ) per residue. The thermal unfolding curves were analyzed by using the two-state model, state $i \leftrightarrow$ state j. Molar ellipticity at each temperature was represented by the following equation:

$$\theta_{obs} = \frac{\theta_i + \theta_j \exp(-\Delta G(T)/RT)}{1 + \exp(-\Delta G(T)/RT)} \quad (14)$$

where $\Delta G(T)$ is the difference in free energy between the states i and j. The ellipticities characteristic for each state were assumed to be a linear function of temperature:

$$\theta(T) = \theta_0 + kT \quad (15)$$

The Gibbs free energy, $\Delta G(T)$, was represented as a function of temperature:

$$\Delta G(T) = \Delta H(T_m)\left(1 - \frac{T}{T_m}\right) - \Delta C_p\left((T_m - T) + T\ln\frac{T}{T_m}\right) \quad (16)$$

where $\Delta H(T_m)$ and ΔC_p are the van't Hoff enthalpy change at the transition temperature, T_m, and the difference in heat capacity before and after the thermal unfolding, respectively. The thermodynamic parameters were estimated in global fits based on experimental points by nonlinear least-squares analysis using the Levenberg–Marquardt algorithm.

Acknowledgements

We thank Drs H. Fukada and T. Kodama for helpful discussions, and Ms H. Sugimoto and Ms S. Hori for their technical assistance. This study was supported in part by a grant from the Japan Foundation for Applied Enzymology (to T. Inui) and by a grant 17300165 (to T. Inui) from the program Grants-in-Aid for Scientific Research (B) of the Ministry of Education, Culture, Sports, Science and Technology of Japan, Tsu City, and Osaka Prefecture. Part of this work was performed under the Cooperative Research Program of Institute for Protein Research, Osaka University.

References

1 Urade Y & Hayaishi O (2000) Biochemical, structural, genetic, physiological, and pathophysiological features of lipocalin-type prostaglandin D synthase. *Biochim Biophys Acta* **1482**, 259–271.
2 Urade Y & Hayaishi O (2000) Prostaglandin D synthase: structure and function. *Vitam Horm* **58**, 89–120.
3 Dumitrascu D (1996) Mast cells as potent inflammatory cells. *Rom J Intern Med* **34**, 159–172.
4 Alving K, Matran R & Lundberg JM (1991) The possible role of prostaglandin D2 in the long-lasting airways vasodilatation induced by allergen in the sensitized pig. *Acta Physiol Scand* **143**, 93–103.
5 Matsuoka T, Hirata M, Tanaka H, Takahashi Y, Murata T, Kabashima K, Sugimoto Y, Kobayashi T, Ushikubi F, Aze Y *et al.* (2000) Prostaglandin D2 as a mediator of allergic asthma. *Science* **287**, 2013–2017.
6 Toh H, Kubodera H, Nakajima N, Sekiya T, Eguchi N, Tanaka T, Urade Y & Hayaishi O (1996) Glutathione-independent prostaglandin D synthase as a lead molecule for designing new functional proteins. *Protein Eng* **9**, 1067–1082.
7 Flower DR, North AC & Sansom CE (2000) The lipocalin protein family: structural and sequence overview. *Biochim Biophys Acta* **1482**, 9–24.
8 Flower DR (1996) The lipocalin protein family: structure and function. *Biochem J* **318**, 1–14.
9 Pervaiz S & Brew K (1987) Homology and structure–function correlations between alpha 1-acid glycoprotein and serum retinol-binding protein and its relatives. *FASEB J* **1**, 209–214.
10 Akerstrom B, Flower DR & Salier JP (2000) Lipocalins: unity in diversity. *Biochim Biophys Acta* **1482**, 1–8.
11 Tanaka T, Urade Y, Kimura H, Eguchi N, Nishikawa A & Hayaishi O (1997) Lipocalin-type prostaglandin D synthase (beta-trace) is a newly recognized type of retinoid transporter. *J Biol Chem* **272**, 15789–15795.
12 Beuckmann CT, Aoyagi M, Okazaki I, Hiroike T, Toh H, Hayaishi O & Urade Y (1999) Binding of biliverdin, bilirubin, and thyroid hormones to lipocalin-type prostaglandin D synthase. *Biochemistry* **38**, 8006–8013.
13 Inui T, Ohkubo T, Urade Y & Hayaishi O (1999) Enhancement of lipocalin-type prostaglandin D synthase enzyme activity by guanidine hydrochloride. *Biochem Biophys Res Commun* **266**, 641–646.
14 Mohri I, Taniike M, Okazaki I, Kagitani-Shimono K, Aritake K, Kanekiyo T, Yagi T, Takikita S, Kim HS, Urade Y *et al.* (2006) Lipocalin-type prostaglandin D synthase is up-regulated in oligodendrocytes in

lysosomal storage diseases and binds gangliosides. *J Neurochem* **97**, 641–651.
15 Kanekiyo T, Ban T, Aritake K, Huang ZL, Qu WM, Okazaki I, Mohri I, Murayama S, Ozono K, Taniike M *et al*. (2007) Lipocalin-type prostaglandin D synthase/beta-trace is a major amyloid beta-chaperone in human cerebrospinal fluid. *Proc Natl Acad Sci USA* **104**, 6412–6417.
16 Inui T, Ohkubo T, Emi M, Irikura D, Hayaishi O & Urade Y (2003) Characterization of the unfolding process of lipocalin-type prostaglandin D synthase. *J Biol Chem* **278**, 2845–2852.
17 Privalov PL (1979) Stability of proteins: small globular proteins. *Adv Protein Chem* **33**, 167–241.
18 Freire E & Biltonen RL (1978) Statistical mechanical deconvolution of thrermal transitions in macromolecules. I. Theory and application to homogeneous systems. *Biopolymers* **17**, 463–479.
19 Manning MC & Woody RW (1989) Theoretical study of the contribution of aromatic side chains to the circular dichroism of basic bovine pancreatic trypsin inhibitor. *Biochemistry* **28**, 8609–8613.
20 Robertson AD & Baldwin RL (1991) Hydrogen exchange in thermally denatured ribonuclease A. *Biochemistry* **30**, 9907–9914.
21 Evans PA, Topping KD, Woolfson DN & Dobson CM (1991) Hydrophobic clustering in nonnative states of a protein: interpretation of chemical shifts in NMR spectra of denatured states of lysozyme. *Proteins* **9**, 248–266.
22 Kuwajima K, Yamaya H & Sugai S (1996) The burst-phase intermediate in the refolding of beta-lactoglobulin studied by stopped-flow circular dichroism and absorption spectroscopy. *J Mol Biol* **264**, 806–822.
23 Hamada D, Segawa S & Goto Y (1996) Non-native alpha-helical intermediate in the refolding of beta-lactoglobulin, a predominantly beta-sheet protein. *Nat Struct Biol* **3**, 868–873.
24 Hamada D & Goto Y (1997) The equilibrium intermediate of beta-lactoglobulin with non-native alpha-helical structure. *J Mol Biol* **269**, 479–487.
25 Ragona L, Fogolari F, Romagnoli S, Zetta L, Maubois JL & Molinari H (1999) Unfolding and refolding of bovine beta-lactoglobulin monitored by hydrogen exchange measurements. *J Mol Biol* **293**, 953–969.
26 Kuwata K, Hoshino M, Forge V, Era S, Batt CA & Goto Y (1999) Solution structure and dynamics of bovine beta-lactoglobulin A. *Protein Sci* **8**, 2541–2545.
27 Uhrinova S, Smith MH, Jameson GB, Uhrin D, Sawyer L & Barlow PN (2000) Structural changes accompanying pH-induced dissociation of the beta-lactoglobulin dimer. *Biochemistry* **39**, 3565–3574.
28 Shimamoto S, Yoshida T, Inui T, Gohda K, Kobayashi Y, Fujimori K, Tsurumura T, Aritake K, Urade Y & Ohkubo T (2007) NMR solution structure of lipocalin-type prostaglandin D synthase: evidence for partial overlapping of catalytic pocket and retinoic acid-binding pocket within the central cavity. *J Biol Chem* **282**, 31373–31379.
29 Hoffmann A, Bachner D, Betat N, Lauber J & Gross G (1996) Developmental expression of murine beta-trace in embryos and adult animals suggests a function in maturation and maintenance of blood–tissue barriers. *Dev Dyn* **207**, 332–343.
30 Plotnikov VV, Brandts JM, Lin LN & Brandts JF (1997) A new ultrasensitive scanning calorimeter. *Anal Biochem* **250**, 237–244.
31 Kidokoro S & Wada A (1987) Determination of thermodynamic functions from scanning calorimetry data. *Biopolymers* **26**, 213–229.
32 Brandts JF, Hu CQ, Lin LN & Mos MT (1989) A simple model for proteins with interacting domains. Applications to scanning calorimetry data. *Biochemistry* **28**, 8588–8596.
33 Honda S, Uedaira H, Vonderviszt F, Kidokoro S & Namba K (1999) Folding energetics of a multidomain protein, flagellin. *J Mol Biol* **293**, 719–732.
34 Privalov GP & Privalov PL (2000) Problems and prospects in microcalorimetry of biological macromolecules. *Methods Enzymol* **323**, 31–62.
35 Freire E (1994) Statistical thermodynamic analysis of differential scanning calorimetry data: structural deconvolution of heat capacity function of proteins. *Methods Enzymol* **240**, 502–530.
36 Sturtevant JM (1987) Biochemical applications of differential scanning calorimetry. *Annu Rev Phys Chem* **38**, 463–488.
37 Privalov PL & Khechinashvili NN (1974) A thermodynamic approach to the problem of stabilization of globular protein structure: a calorimetric study. *J Mol Biol* **86**, 665–684.
38 Freire E, Murphy KP, Sanchez-Ruiz JM, Galisteo ML & Privalov PL (1992) The molecular basis of cooperativity in protein folding. Themodynamic dissection of interdomain interactions in phosphoglycerate kinase. *Biochemistry* **31**, 250–256.
39 Griko YV, Freire E, Privalov G, van Dael H & Privalov PL (1995) The unfolding thermodynamics of c-type lysozymes: a calorimetric study of the heat denaturation of equine lysozyme. *J Mol Biol* **252**, 447–459.
40 Privalov PL & Makhatadze GI (1992) Contribution of hydration and non-covalent interactions to the heat capacity effect on protein unfolding. *J Mol Biol* **224**, 715–723.